



The Chemical Composition of NGC 5824, a Globular Cluster without Iron Spread but with an Extreme Mg–Al Anticorrelation*

Alessio Mucciarelli^{1,2} , Emilio Lapenna^{1,2} , Francesco R. Ferraro^{1,2} , and Barbara Lanzoni^{1,2} 

¹Dipartimento di Fisica & Astronomia, Università degli Studi di Bologna, via Gobetti 93/2, I-40129, Bologna, Italy

²INAF—Osservatorio di Astrofisica e Scienza dello Spazio, via Gobetti 93/3, I-40129, Bologna, Italy

Received 2018 February 12; revised 2018 March 25; accepted 2018 March 26; published 2018 May 24

Abstract

NGC 5824 is a massive Galactic globular cluster suspected to have an intrinsic spread in its iron content, according to the strength of the calcium triplet lines. We present chemical abundances of 117 cluster giant stars using high-resolution spectra acquired with the multi-object spectrograph FLAMES. The metallicity distribution of 87 red giant branch stars is peaked at $[\text{Fe}/\text{H}] = -2.11 \pm 0.01$ dex, while that derived from 30 asymptotic giant branch stars is peaked at $[\text{Fe}/\text{H}] = -2.20 \pm 0.01$ dex. Both the distributions are compatible with a null spread, indicating that this cluster did not retain the ejecta of supernovae. The small iron abundance offset between the two groups of stars is similar to the abundances already observed among red and asymptotic giant branch stars in other clusters. The lack of intrinsic iron spread rules out the possibility that NGC 5824 is the remnant of a disrupted dwarf galaxy, as previously suggested. We also find evidence of the chemical anomalies usually observed in globular clusters, namely the Na–O and the Mg–Al anticorrelations. In particular, NGC 5824 exhibits a huge range of $[\text{Mg}/\text{Fe}]$ abundance, observed in only a few metal-poor and/or massive clusters. We conclude that NGC 5824 is a normal globular cluster, without spread in $[\text{Fe}/\text{H}]$ but with an unusually large spread in $[\text{Mg}/\text{Fe}]$, possibly due to an efficient self-enrichment driven by massive asymptotic giant branch stars.

Key words: globular clusters: individual (NGC 5824) – stars: abundances – techniques: spectroscopic

Supporting material: machine-readable tables

1. Introduction

The majority of the Galactic globular clusters (GCs) studied so far through high-resolution spectroscopy reveal two chemical signatures, usually considered as the key features to define a stellar system as a GC: (1) a very small star-to-star scatter in their iron abundance, compatible, within the uncertainties, with a null spread (see, e.g., Carretta et al. 2009a; Willman & Strader 2012); (2) the presence of star-to-star variations in the chemical abundances of some light elements, structured in some well-defined patterns, such as the Na–O and Mg–Al anticorrelations (see, e.g., Carretta et al. 2009b, 2009c; Meszaros et al. 2015; Pancino et al. 2017).

The first observation indicates that GCs were not massive enough to retain in their gravitational well the high-velocity ejecta of supernovae. The second observation instead is interpreted as the signature of the retaining/recycling of the low-velocity ejecta of some polluter stars where high-temperature proton-capture cycles (CNO, NeNa, and MgAl chains) occurred. While the details of this self-enrichment process are still unclear and under debate (see, e.g., the critical discussions by Bastian & Lardo 2015 and Renzini et al. 2015), the presence of chemically distinct stellar populations in GCs is now widely recognized and accepted.

While the Na–O anticorrelation has been detected in almost all old GCs studied so far (at least in those with statistically significant samples³), some undeniable exceptions to the first observation quoted above are known. There are three massive stellar systems, usually labeled as GCs according to their

appearance and brightness profile, that show large metallicity distributions: Omega Centauri in the Galactic Halo (Johnson & Pilachowski 2010; Marino et al. 2011b; Pancino et al. 2011), Terzan 5 in the Galactic Bulge (Ferraro et al. 2009; Origlia et al. 2011, 2013; Massari et al. 2014), and M54 in the Sagittarius dwarf galaxy (Brown et al. 1999; Bellazzini et al. 2008; Carretta et al. 2010a, 2010b; Mucciarelli et al. 2017a). The first two stellar systems have multimodal $[\text{Fe}/\text{H}]$ distributions, covering a range of ~ 1 dex, while the metallicity distribution of M54, once the contamination of the Sagittarius stars has been taken into account, is significantly smaller than those of Omega Centauri and Terzan 5. Even if characterized by the largest metallicity distributions observed so far among GC-like systems, these three systems cannot be easily explained within the same framework: Omega Centauri is usually interpreted as the remnant of a disrupted dwarf spheroidal galaxy (Bekki & Freeman 2003), Terzan 5 is likely the fossil relic of one of the primordial structures that contributed to building up the Galactic Bulge (Ferraro et al. 2016), while M54, due to its position coincident with the center of the Sagittarius galaxy and the strong difference between its dispersion velocity profile and that of Sagittarius, should be a GC formed independently by the true nucleus of the galaxy and decayed to its present-day position due to dynamical friction (as demonstrated by Bellazzini et al. 2008).

Recently, other GCs have been proposed to have an intrinsic iron spread (but smaller than those observed in the three stellar systems quoted above). Small intrinsic $[\text{Fe}/\text{H}]$ scatters (of the order of 0.1 dex), based on both low- and high-resolution spectroscopy, have been claimed for M22 (Marino et al. 2009), NGC 3201 (Simmerer et al. 2013), M2 (Yong et al. 2014), NGC 5824 (Da Costa et al. 2014, hereafter DC14), NGC 5286 (Marino et al. 2015), and M19 (Johnson et al. 2016). For most

* Based on observations collected at the ESO-VLT under the program 095. D-0290.

³ We recall the case of Ruprecht 106, which does not show chemical anomalies in the light elements from the analysis of nine stars (Villanova et al. 2013).

of these clusters (such as M2, M22, NGC 5286, and M19), spreads in the s-process and C+N+O abundances (with $[s/Fe]$ and C+N+O abundance ratios increasing with $[Fe/H]$) have been detected, similar to that observed in Omega Centauri (no information about s-process element abundances is available so far for Terzan 5 and M54⁴). The similarities (but to a lower extent) with Omega Centauri have suggested that these clusters could be the remnants of dwarf galaxies accreted from our Galaxy (see, e.g., the discussion in Marino et al. 2015).

Even if fascinating, this hypothesis needs to be supported by extensive and robust spectroscopic studies, because several different effects can mimic a spurious iron spread. In the case of NGC 3201, the iron spread originally proposed by Simmerer et al. (2013) was found to be due to the inclusion in the sample of some asymptotic giant branch (AGB) stars that show systematic underabundances of $[Fe I/H]$ (see Lapenna et al. 2014) and hence it was erroneously interpreted as a metal-poor tail in the cluster metallicity distribution (Mucciarelli et al. 2015a). In the remote GC NGC 2419 (the GC with the largest $[Mg/Fe]$ spread, having stars with $[Mg/Fe]$ extending down to ~ -1 dex) the strength of the Ca II triplet lines provides a wide metallicity distribution (see Ibata et al. 2011). However, this iron spread is artificial because the strength of the Ca II triplet lines (at a constant Fe and Ca abundance) increases significantly in those stars characterized by a relevant depletion in Mg, Mg being one of the most important electron donors in the atmospheres of giant stars (Mucciarelli et al. 2012). Also the case of M22 has been revised by Mucciarelli et al. (2015b), demonstrating that the use of photometric gravities (instead of spectroscopic ones) leads to a narrow iron distribution, compatible with a null intrinsic spread, when Fe II lines are measured (while the use of spectroscopic gravities provides two broad metallicity distributions but also implies unrealistic and too low stellar masses). A similar approach has been applied by Lardo et al. (2016) to M2, thus reducing the iron spread claimed for this cluster by Yong et al. (2014).

In this paper we focus our attention on the outer halo GC NGC 5824, another cluster for which a modest iron spread was claimed. First, Saviane et al. (2012) suggested a possible metallicity spread based on metallicity inferred from the strength of the Ca II triplet lines of 17 stars, subsequently confirmed by DC14, who adopted the same technique for a sample of 108 red giant branch (RGB) cluster stars. The $[Fe/H]$ distribution derived by DC14 has an average value of -2.01 ± 0.01 dex with an observed spread of 0.07 dex. DC14 proposed that also NGC 5824 could be another case of a remnant of a disrupted dwarf galaxy.

Using the Magellan II Telescope, Roederer et al. (2016, hereafter Ro16) measured the chemical composition of 26 stars using the Michigan/Magellan Fiber System (with a spectral resolution of $\sim 34,000$ and a spectral coverage of 4425–4635 Å) and that of two stars using the MIKE spectrograph (spectral resolution of $\sim 40,000$ and coverage of ~ 3350 –9150 Å). The total sample provides an average $[Fe/H]$ abundance of -2.38 ± 0.01 dex ($\sigma = 0.08$ dex) from Fe I lines and of -1.94 ± 0.02 dex ($\sigma = 0.08$ dex) from Fe II lines. The observed dispersions from the two iron distributions are

compatible with a null spread, even if Ro16 noted that their observed targets are in the brightest portion of the RGB where the corresponding targets of DC14 provide a small dispersion (while a larger dispersion is found for the faintest stars). Ro16 concluded that their high-resolution spectroscopic sample may not be adequate to provide a conclusive answer about a possible iron spread in this cluster.

In this paper we investigate the chemical composition of NGC 5824 using a sample of high-resolution spectra collected with FLAMES at the Very Large Telescope for a total of 117 member stars.

2. Observations

The observations have been collected under the program 095.D-0290 (PI: Mucciarelli) and performed during the night of 2015 May 28 with the multi-object spectrograph FLAMES (Pasquini et al. 2000) at the Very Large Telescope of ESO in the GIRAFFE+UVES combined mode, allowing the simultaneous allocation of 132 mid-resolution GIRAFFE fibers and 8 high-resolution UVES (Dekker et al. 2000) fibers. The adopted setups are GIRAFFE HR21 (with a spectral coverage of ~ 8480 –9000 Å and a spectral resolution of 18,000) and UVES Red Arm 580 (with a spectral coverage of ~ 4800 –6800 Å and a spectral resolution of 45,000). Two configurations of targets have been defined: the first has been observed with four exposures of 45 minutes each and the second with five exposures of 45 minutes each. The targets have been selected from the WFPC2@HST photometric catalog by Sanna et al. (2014), picking only giant stars predicted to be not contaminated within the FLAMES fiber diameter by neighboring stars with brighter or comparable magnitudes. In the target allocation procedure the highest priority has been attributed to stars already observed: the UVES fibers were allocated to stars already observed by DC14 and Ro16, and the GIRAFFE fibers to the remaining DC14 targets for which their membership has been already established. Most of the targets have been allocated within ~ 350 arcsec from the cluster center; at larger radii the color–magnitude diagram (CMD) is dominated by field stars and the cluster sequences are barely recognizable. The residual fibers have been allocated to giant stars in the external regions, in order to have a sample of surrounding field stars for the identification of possible Galactic interlopers among the stars observed close to the cluster. A total of 211 stars have been observed (205 with GIRAFFE and 6 with UVES). Eighty-eight of them are in common with DC14, while 23 are in common with Ro16 (all in common with DC14). Finally, about 20 GIRAFFE fibers and two UVES fibers have been dedicated to observe empty sky regions in order to sample the sky background.

The spectra have been reduced using the dedicated ESO pipelines that perform bias subtraction, flat-fielding, wavelength calibration, one-dimensional spectral extraction, and (only for the UVES spectra) order merging. For each exposure, the spectra of the sky regions have been combined together and the derived master-sky spectrum subtracted from each individual stellar spectrum. The latter have been corrected for the corresponding heliocentric radial velocity (RV) as explained in Section 3 and finally the spectra of each target coadded together, reaching a signal-to-noise ratio (S/N) per pixel from ~ 70 for the faintest GIRAFFE targets ($V \sim 17.8$) to

⁴ Note that Carretta et al. (2014) quoted the average $[s/Fe]$ abundance ratios measured in the UVES stars of M54 already discussed in Carretta et al. (2010a, 2010b) but not the abundances for the individual stars. This makes it impossible to understand whether M54 also shows the same behavior of $[s/Fe]$ with $[Fe/H]$.

Table 1
Main Information on the Spectroscopic Targets of NGC 5824

| ID | ID _{DC14} | R.A. (J2000) | Decl. (J2000) | <i>U</i> | <i>V</i> | RV _{hel} (km s ⁻¹) | Sequence |
|-------|--------------------|-----------------|------------------|----------|----------|--|----------|
| 8953 | ... | 226.1162748 | -33.1975713 | 18.464 | 17.032 | -24.30 ± 0.10 | RGB |
| 10222 | 62000309 | 226.0997769 | -33.1493884 | 18.503 | 17.530 | -22.10 ± 0.35 | AGB |
| 10647 | ... | 226.0940622 | -33.1212687 | 17.901 | 15.773 | -33.00 ± 0.25 | RGB |
| 10967 | ... | 226.0904849 | -32.9280129 | 18.218 | 15.972 | -26.70 ± 0.06 | RGB |
| 11276 | 42007983 | 226.0868524 | -33.0699666 | 18.354 | 17.224 | -28.60 ± 0.12 | AGB |
| 11730 | ... | 226.0817615 | -32.9692462 | 18.085 | 16.306 | -30.30 ± 0.06 | RGB |
| 12035 | ... | 226.0783242 | -33.0665547 | 18.586 | 17.645 | -28.10 ± 0.03 | AGB |
| 12077 | ... | 226.0779387 | -33.0395730 | 18.033 | 16.367 | -26.30 ± 0.03 | AGB |
| 12898 | 42011701 | 226.0699481 | -33.0487649 | 19.097 | 17.890 | -29.10 ± 0.14 | RGB |
| 13068 | 42008963 | 226.0685097 | -33.0643136 | 18.780 | 17.703 | -23.80 ± 0.11 | RGB |
| 13705 | ... | 226.0629148 | -33.1187793 | 18.379 | 17.165 | -28.00 ± 0.06 | AGB |
| 13793 | ... | 226.0623981 | -32.9325047 | 18.411 | 16.916 | -30.40 ± 0.04 | RGB |
| 13894 | 11001198 | 226.0614866 | -33.0429962 | 18.136 | 16.463 | -23.80 ± 0.06 | RGB |
| 14000 | 62000027 | 226.0608134 | -33.1705065 | 18.363 | 16.658 | -26.80 ± 0.05 | RGB |

Note. Identification numbers (from Sanna et al. 2014 and from DC14), coordinates, magnitudes, heliocentric radial velocities, and evolutionary sequences for all the member stars.

(This table is available in its entirety in machine-readable form.)

~260 for the brightest ones ($V \sim 15.4$). For the UVES spectra an S/N per pixel of ~50 is reached.

3. Radial Velocities

RVs have been measured adopting the standard cross-correlation method as implemented in the IRAF task FXCOR. As the template spectrum we adopted a synthetic spectrum calculated with the SYNTH code (see Sbordone et al. 2004) and convolved with a Gaussian profile in order to reproduce the instrumental profile. Before measuring the RV on the photospheric lines, we checked the correctness of the wavelength calibration by measuring the position of some sky emission lines: no significant offset in the zero-point of the wavelength calibration is found for either GIRAFFE or UVES spectra.

For each target, the measurement of RV has been performed on the spectra of individual exposures, and then the final heliocentric RV has been computed as the average of the individual values. This approach allows us to detect possible binary stars, at least those stars with RV variations detectable within the same night. We identified only one star (namely #29580) that shows a dispersion of the average RV significantly larger than those measured in stars of similar magnitude. This star, even if a likely cluster member according to its median RV and the small distance from the cluster center (~60 arcsec), has been excluded from the following chemical analysis.

Table 1 lists for all the targets the final heliocentric RVs computed as the non-weighted mean of the individual measurements; the quoted uncertainties have been computed as the dispersion of the mean normalized to the root mean square of the number of exposures used.

For the 88 targets in common with DC14 an average RV difference (i.e., our study - DC14) of $+2.5 \pm 1.1$ km s⁻¹ ($\sigma = 10.1$ km s⁻¹) is found, where the dispersion is dominated by the uncertainties in the DC14 RVs, due to the lower spectral resolution ($R \sim 2500$). For the 23 stars in common with Ro16 we found $+0.7 \pm 0.2$ km s⁻¹ ($\sigma = 0.8$ km s⁻¹).

Figure 1 shows the behavior of the heliocentric RVs of all the targets as a function of the distance from the cluster center quoted by Sanna et al. (2014). As can be seen, a group of stars with RV clumped around ~ -26 km s⁻¹ is clearly recognizable out to ~350 arcsec, while for larger radii the sample shows a significant RV dispersion. The gray points are the stars selected as cluster members according to their RV and [Fe/H] (see Section 6). The position of the candidate binary star is shown by a square symbol.

4. Atmospheric Parameters

The atmospheric parameters have been determined using photometric information. The magnitudes of the catalog by Sanna et al. (2014) have been reported in the standard Johnson photometric system using the stars in common with the catalog of photometric standard stars by P. B. Stetson.⁵ Effective temperatures (T_{eff}) have been computed by means of the $(U - V)_0 - T_{\text{eff}}$ transformation by Alonso et al. (1999, 2001) and by adopting the color excess $E(B - V) = 0.14$ mag (Ferraro et al. 1999). The extinction coefficients are from McCall (2004). Because of the dependence of the $(U - V)_0 - T_{\text{eff}}$ relation on the metallicity, we guessed a value of metallicity $[\text{Fe}/\text{H}] = -2.0$ dex (according to DC14 and Ro16) for all the targets. After a first determination of the chemical abundances, T_{eff} have been refined using the proper metallicity of each star.

Surface gravities ($\log g$) have been estimated using the Stefan-Boltzmann relation, assuming the photometric T_{eff} , the bolometric corrections estimated according to Alonso et al. (1999), and the true distance modulus quoted by Ferraro et al. (1999) ($(m - M)_0 = 17.53$ mag). In the first determination of $\log g$, we assumed a stellar mass of $0.75 M_{\odot}$; subsequently we attributed a stellar mass of $0.65 M_{\odot}$ to the member stars labeled as AGB stars according to their position in the $V - (U - V)$ CMD (see Section 6). Note that an incorrect attribution of a cluster star to an evolutionary sequence has a negligible impact on the derived abundances: a difference of $0.1 M_{\odot}$ in stellar mass

⁵ <http://www.cadc-ccda.hia-ihp.nrc-cnrc.gc.ca/en/community/STETSON/standards/>

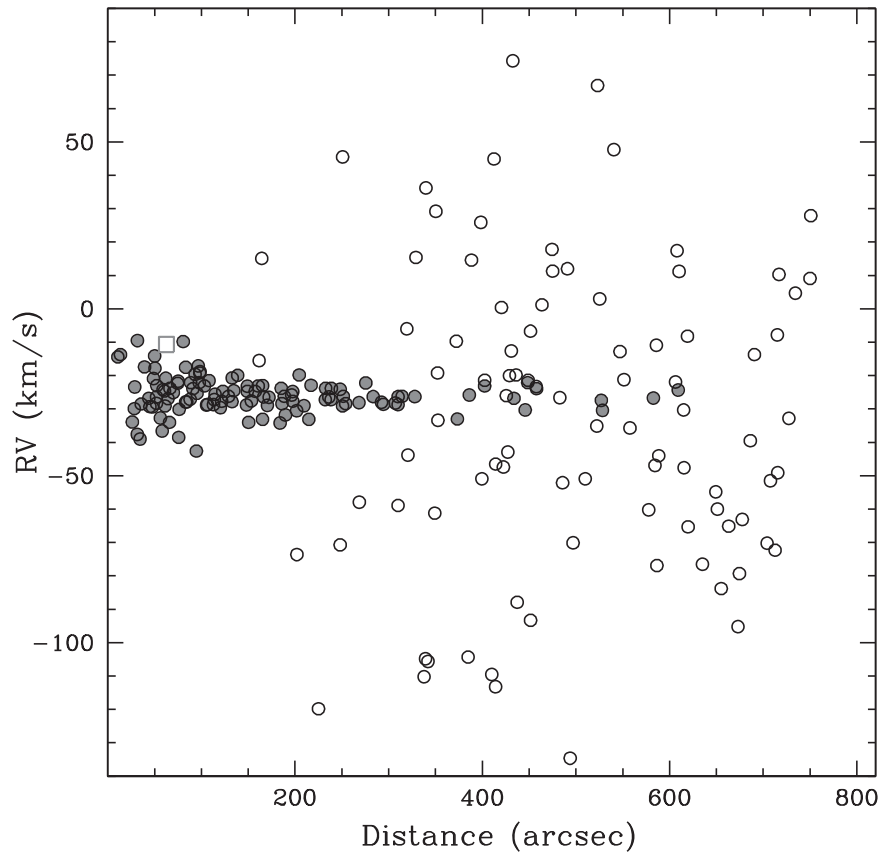


Figure 1. Behavior of RV as a function of the distance from the cluster center for all the observed targets of NGC 5824. Gray filled points are the stars flagged as cluster members according to their RV and $[\text{Fe}/\text{H}]$. The gray empty square indicates a candidate binary star.

leads to a variation in $\log g$ of ~ 0.06 , corresponding to a variation in the $[\text{Fe}/\text{H}]$ abundances of 0.01 dex or less.

Due to the small (~ 15) number of Fe I lines available for the GIRAFFE targets (which are the majority of the sample), microturbulent velocities (v_t) derived spectroscopically could be highly uncertain and we prefer to adopt the $\log g - v_t$ calibration provided by Kirby et al. (2009). Although the number of lines is small, we checked for most of the stars that the adopted v_t does not provide a significant trend between iron abundance and line strength. Only for a few stars do we find a significant slope (at a level of 3σ or more), and we change the value of v_t in order to erase this trend.

The six stars observed with UVES allow us to perform some sanity checks on the atmospheric parameters adopted for the analysis. The atmospheric parameters have been derived spectroscopically according to three criteria: (i) no trend between Fe I abundance and excitation potential (to constrain T_{eff}); (ii) no trend between Fe I abundance and line strength (to constrain v_t); (iii) same abundance from Fe I and Fe II lines (to constrain $\log g$). The spectroscopic T_{eff} agree well with the photometric ones, with an average difference (spectroscopic minus photometric) of -47 K ($\sigma = 29$ K), as do the microturbulent velocities (the spectroscopic ones are on average lower than those obtained with the calibration of Kirby et al. (2009) by -0.2 km s $^{-1}$, $\sigma = 0.07$ km s $^{-1}$). Finally, the spectroscopic gravities are lower by -0.2 dex ($\sigma = 0.03$ dex), due to the small difference (~ -0.1 dex) between $[\text{Fe I}/\text{H}]$ and $[\text{Fe II}/\text{H}]$ obtained with the photometric $\log g$. The average difference in $[\text{Fe I}/\text{H}]$ derived from spectroscopic and photometric parameters is -0.03 dex ($\sigma = 0.04$ dex),

suggesting that the adopted parameters are not affected by any significant bias.

5. Chemical Analysis

Abundances of Fe, Al, and Mg have been derived for all the targets, while abundances of O and Na have been determined only for the UVES targets, because no O and Na lines are available in the GIRAFFE HR21 setup. In particular, Fe I lines are available for both UVES and GIRAFFE targets, while Fe II lines have been measured only in UVES spectra (because no Fe II lines are in the HR21 GIRAFFE grating).

For all these elements, the chemical analysis is based on one-dimensional, plane-parallel model atmospheres calculated with the code ATLAS9 (Castelli 2005), adopting an α -enhanced chemical mixture and without the inclusion of the approximate overshooting in the calculation of the convective flux. The derived abundance ratios are referred to the solar abundances of Grevesse & Sauval (1998) except for O, for which we adopted the solar value of Caffau et al. (2011).

The abundances of Fe, Na, and Al have been calculated from the measured equivalent widths of metallic lines using the code GALA (Mucciarelli et al. 2013), based on the WIDTH9 software originally developed by R. L. Kurucz (see Castelli 2005, for details). We selected transitions predicted to be unblended at the resolution of UVES and the HR21 GIRAFFE setup. The atomic data are from the Kurucz/Castelli linelist,⁶ improved with new atomic data for some lines of interest (we refer the reader to

⁶ <http://www.oact.inaf.it/castelli/castelli/linelists.html>

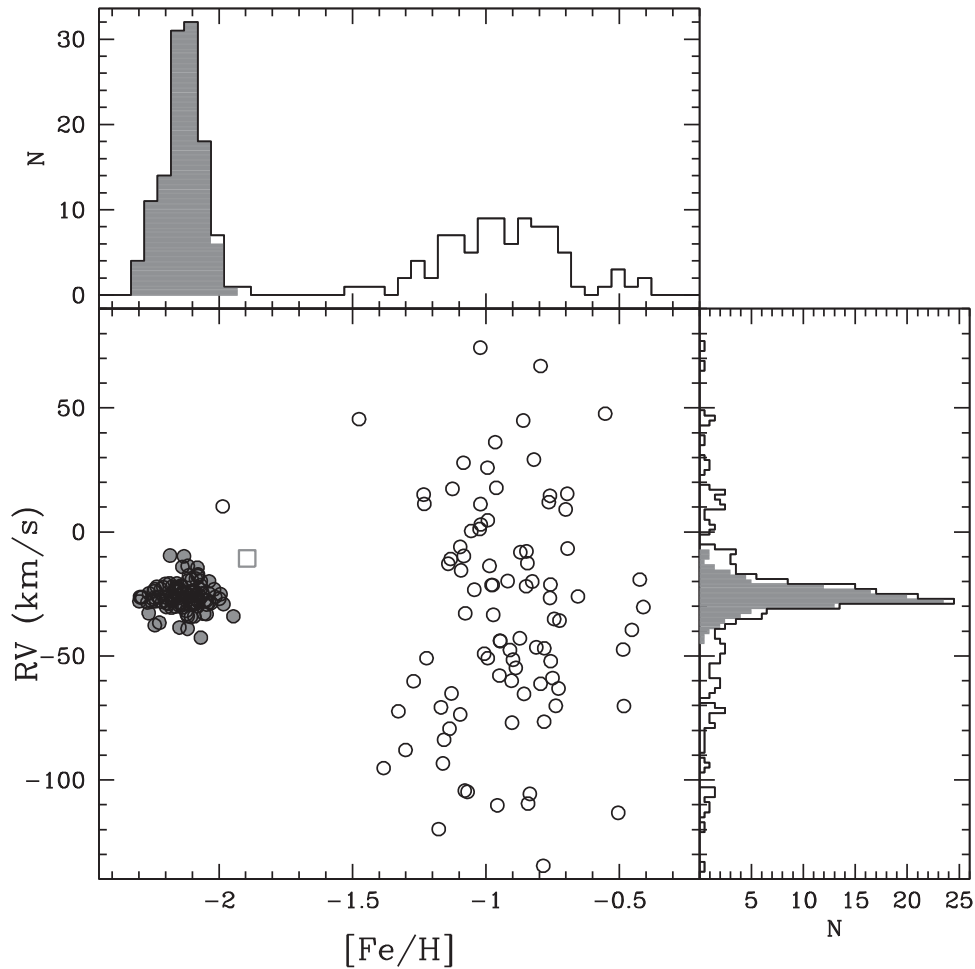


Figure 2. The main panel shows the behavior of the RV of the observed stars as a function of $[\text{Fe}/\text{H}]$ (same symbols as Figure 1). The histograms of $[\text{Fe}/\text{H}]$ and RV distributions are also plotted (the gray shaded histograms include only cluster member stars).

Table 2

Wavelength, Species, Oscillator Strength, and Excitation Potential of the Transitions Used

| Wavelength (Å) | Species | Log gf | χ (eV) | Instrument |
|----------------|---------|----------|-------------|------------|
| 4859.741 | Fe I | -0.764 | 2.875 | UVES |
| 4882.143 | Fe I | -1.640 | 3.417 | UVES |
| 4907.732 | Fe I | -1.840 | 3.430 | UVES |
| 4917.230 | Fe I | -1.160 | 4.191 | UVES |
| 4924.770 | Fe I | -2.114 | 2.279 | UVES |
| 4938.814 | Fe I | -1.077 | 2.875 | UVES |
| 4950.106 | Fe I | -1.670 | 3.417 | UVES |
| 4969.917 | Fe I | -0.710 | 4.217 | UVES |
| 4985.253 | Fe I | -0.560 | 3.929 | UVES |
| 4985.547 | Fe I | -1.331 | 2.865 | UVES |
| 4993.358 | Fe II | -3.620 | 2.807 | UVES |
| 5001.863 | Fe I | -0.010 | 3.882 | UVES |
| 5002.793 | Fe I | -1.530 | 3.396 | UVES |
| 5014.942 | Fe I | -0.303 | 3.943 | UVES |

Note. The last column indicates whether the transition has been measured in the UVES or GIRAFFE spectra.

(This table is available in its entirety in machine-readable form.)

Mucciarelli et al. (2017b) for a detailed description of the linelist). Table 2 lists the atomic data (wavelength, oscillator strength, and excitation potential) for all the transitions used.

Al abundances from GIRAFFE targets are derived from the doublet at 8772–8773 Å, while those from UVES targets are from the doublet at 6696–6698 Å. For some stars these lines are too weak to be detected, due to the low Al abundances (see Section 8), and only upper limits can be provided by adopting the abundance corresponding to an EW equal to three times the uncertainty calculated according to the formula of Cayrel (1988).

The Na abundances for the UVES targets have been obtained from the doublets 5682–5688 Å and 6154–6160 Å and corrected for departures from local thermodynamic equilibrium according to Gratton et al. (1999).

The abundances of Mg for the GIRAFFE targets have been derived from the Mg I line at 8806 Å by using spectral synthesis, in order to properly account for the profile of this strong line, which can have significant wings. In particular, the abundances have been obtained using our own code SALVADOR, which performs a χ^2 -minimization between the observed spectra, and a grid of synthetic spectra calculated on the fly with the spectral synthesis code SYNTHÉ. For the UVES targets, Mg abundances have been obtained from the measurement of the EW of the Mg I line at 5711 Å. The Mg abundances for the GIRAFFE targets have been decreased by -0.28 dex in order to match the peak of the $[\text{Mg}/\text{Fe}]$ distribution for the GIRAFFE stars with the highest $[\text{Mg}/\text{Fe}]$ derived for the UVES targets. Offsets between the Mg abundances derived from the line at 8806 Å and those derived from optical lines

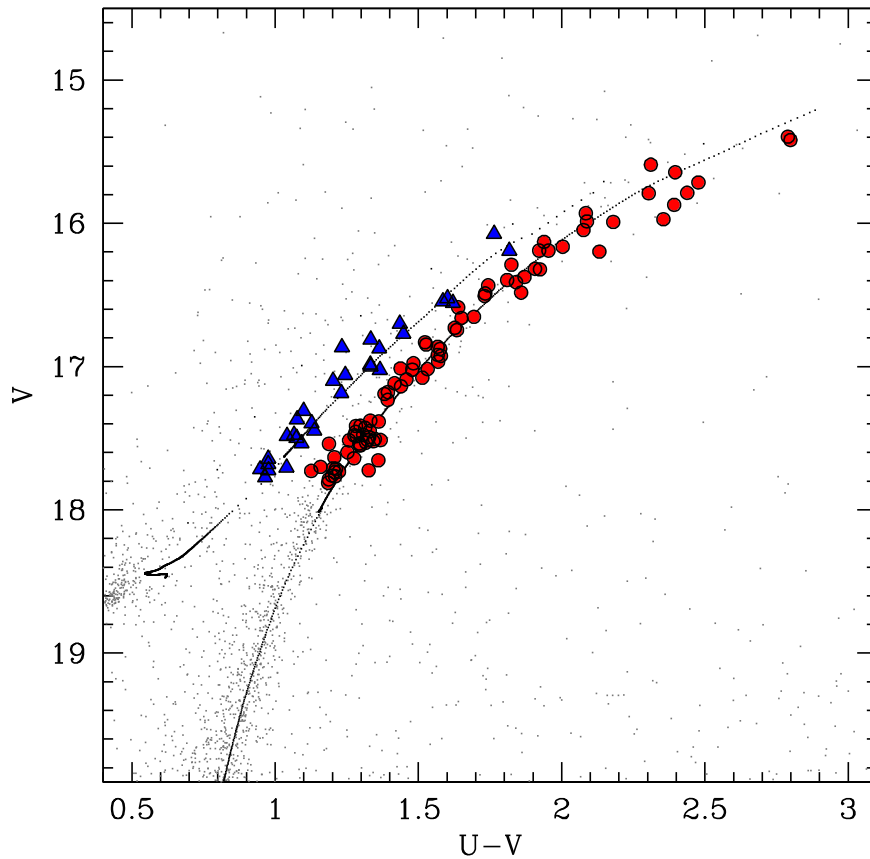


Figure 3. Position of the member stars in the $V-(U-V)$ CMD (Sanna et al. 2014): RGB and AGB stars are plotted as red circles and blue triangles, respectively. The best-fit theoretical isochrone from the BaSTI database (13 Gyr, $Z = 0.0006$, α -enhanced chemical mixture, Pietrinferni et al. 2006) is plotted as a reference.

Table 3
Atmospheric Parameters and Abundance Ratios for the UVES Targets of NGC 5824

| ID | T_{eff} (K) | Log g | v_t (km s^{-1}) | [Fe/H] (dex) | [O/Fe] (dex) | [Na/Fe] (dex) | [Mg/Fe] (dex) | [Al/Fe] (dex) |
|-------|-------------------------|---------|---------------------------------|------------------|------------------|------------------|------------------|------------------|
| 20836 | 4270 | 0.77 | 2.0 | -2.07 ± 0.06 | -1.99 ± 0.08 | 0.08 ± 0.03 | 0.48 ± 0.08 | <0.21 |
| 24182 | 4252 | 0.83 | 1.9 | -2.16 ± 0.06 | -1.93 ± 0.09 | 0.09 ± 0.04 | 0.50 ± 0.02 | <0.28 |
| 26034 | 4238 | 0.69 | 2.0 | -2.14 ± 0.06 | -2.00 ± 0.08 | 0.08 ± 0.08 | 0.23 ± 0.03 | 1.08 ± 0.03 |
| 27416 | 4344 | 0.90 | 1.9 | -2.14 ± 0.06 | -2.01 ± 0.09 | 0.09 ± 0.06 | 0.38 ± 0.03 | <0.33 |
| 31793 | 4313 | 0.88 | 1.9 | -2.15 ± 0.06 | -1.96 ± 0.08 | 0.08 ± 0.03 | 0.03 ± 0.05 | 1.22 ± 0.03 |
| 35432 | 4239 | 0.78 | 2.0 | -2.17 ± 0.06 | -1.95 ± 0.08 | 0.08 ± 0.06 | -0.24 ± 0.05 | 1.18 ± 0.03 |

have been already found in other analysis (see, e.g., Mucciarelli et al. 2017a). Note that we are interested mainly in the star-to-star variations of [Mg/Fe] in this cluster and not in the absolute value of the abundances.

The uncertainties in any abundance ratio have been calculated by summing in quadrature the errors arising from the measurement procedure (EWs or spectral fitting) and from the atmospheric parameters.

(1) *Uncertainties due to EWs*—The errors in abundance due to the EW measurements have been computed as the dispersion of the mean normalized to the root mean square of the number of lines used. When only one line is available, the uncertainty is estimated considering the error in EW provided by DAOSPEC.

(2) *Uncertainties due to spectral fitting*—The uncertainties in the fitting procedure have been estimated using Monte Carlo simulations. For different values of S/N, corresponding to the range of S/N covered by the GIRAFFE targets, samples of 500 synthetic spectra at the same spectral resolution and pixel size as the GIRAFFE spectra and with the inclusion of Poissonian noise have been created and analyzed with the same fitting procedure used for the observed spectra. The dispersion of the derived abundance distribution is assumed as the 1σ uncertainty associated with the abundance from spectra with that S/N. The derived uncertainties in the fitting procedure range from ~ 0.01 dex for $S/N = 260$ to ~ 0.07 dex for $S/N = 70$ for the Mg I line at 8806 \AA measured in the GIRAFFE targets. The typical uncertainty for the O abundance is about 0.05 dex.

Table 4
Atmospheric Parameters and Abundance Ratios for the GIRAFFE Targets of NGC 5824

| ID | T_{eff} (K) | Log g | v_t (km s^{-1}) | [Fe/H] (dex) | [Mg/Fe] (dex) | [Al/Fe] (dex) |
|-------|-------------------------|---------|---------------------------------|------------------|------------------|------------------|
| 8953 | 4578 | 1.4 | 1.8 | -2.13 ± 0.08 | 0.37 ± 0.07 | <0.02 |
| 10222 | 4955 | 1.7 | 1.7 | -2.14 ± 0.07 | 0.51 ± 0.10 | <0.25 |
| 10647 | 4265 | 0.7 | 2.0 | -2.06 ± 0.07 | 0.52 ± 0.06 | <-0.03 |
| 10967 | 4220 | 0.7 | 2.0 | -2.15 ± 0.05 | 0.47 ± 0.06 | 0.62 ± 0.04 |
| 11276 | 4787 | 1.5 | 1.8 | -2.20 ± 0.07 | 0.68 ± 0.08 | <0.32 |
| 11730 | 4382 | 1.0 | 1.9 | -2.20 ± 0.06 | 0.41 ± 0.06 | <-0.09 |
| 12035 | 4981 | 1.8 | 1.7 | -2.25 ± 0.07 | 0.46 ± 0.10 | <0.50 |
| 12077 | 4415 | 1.0 | 1.9 | -2.29 ± 0.07 | 0.07 ± 0.06 | 1.25 ± 0.06 |
| 12898 | 4747 | 1.8 | 1.7 | -1.98 ± 0.07 | 0.33 ± 0.08 | <0.42 |
| 13068 | 4846 | 1.8 | 1.7 | -2.10 ± 0.07 | 0.26 ± 0.09 | <0.54 |
| 13705 | 4707 | 1.5 | 2.1 | -2.30 ± 0.06 | 0.49 ± 0.07 | <0.32 |
| 13793 | 4532 | 1.3 | 1.8 | -2.14 ± 0.07 | 0.48 ± 0.07 | <0.01 |
| 13894 | 4420 | 1.1 | 1.9 | -2.16 ± 0.07 | 0.51 ± 0.06 | <-0.01 |
| 14000 | 4408 | 1.1 | 1.9 | -2.18 ± 0.07 | 0.31 ± 0.06 | 1.26 ± 0.06 |

(This table is available in its entirety in machine-readable form.)

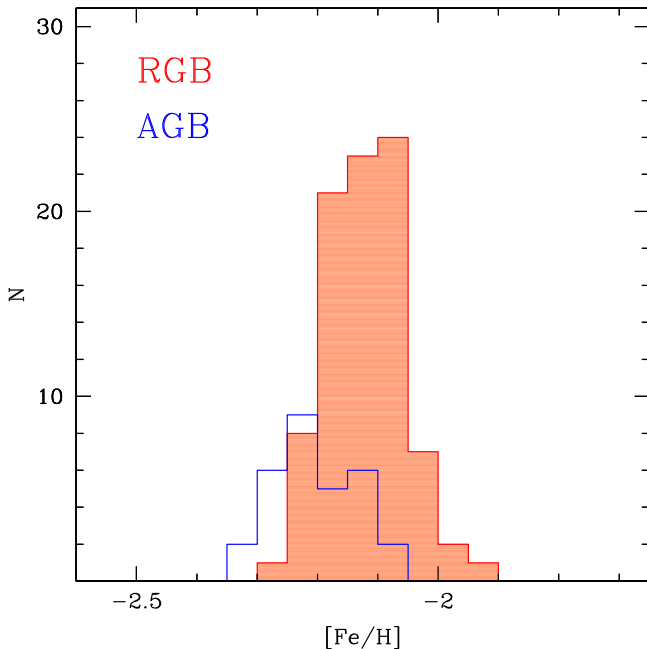


Figure 4. [Fe/H] distributions derived from this study for RGB and AGB stars, the red and blue histograms respectively.

- (3) *Uncertainties due to the atmospheric parameters*—These uncertainties are computed by varying only one parameter each time by the corresponding error, keeping the other ones fixed and repeating the analysis. According to the photometric uncertainties, we estimated internal errors of about 40 K in T_{eff} , 0.1 in $\log g$, and 0.1 km s^{-1} in v_t . Note that we are mainly interested in the internal uncertainties in the atmospheric parameters because the main goal of this study is investigate possible intrinsic star-to-star scatter.

6. Membership

We identified likely cluster member stars according to their RV and [Fe/H]. Figure 2 shows the position of the observed targets in the RV–[Fe/H] plane. Stars belonging to NGC 5824

are easily identifiable as a clump of stars around $\text{RV} \sim -25 \text{ km s}^{-1}$ and $[\text{Fe}/\text{H}] \sim -2.1$ dex. The surrounding field stars show a large RV distribution peaked at values similar to those of the cluster stars but with metallicities larger than $[\text{Fe}/\text{H}] \sim -1.5$ dex and peaked at ~ -0.9 dex. We consider member stars to be those with $[\text{Fe}/\text{H}]$ between -2.35 and -1.90 dex and with RV between -50 and 0 km s^{-1} (and marked as gray circles in Figure 2).

A total of 117 cluster member stars are identified. All the main information (coordinates, magnitudes, RVs) on these stars is listed in Table 1. Note that 11 of them are located at a distance from the cluster center larger than 350 arcsec, where the sample is dominated by Galactic field stars. However, their metallicity is clearly different from that of the surrounding field and this provides their membership of the cluster. The mean heliocentric RV of this sample is $-26.0 \pm 0.5 \text{ km s}^{-1}$ ($\sigma = 5.4 \text{ km s}^{-1}$), in good agreement with those quoted by DC14 and Ro16. According to the distance in the V –($U - V$) CMD to the best-fit theoretical isochrone (see Sanna et al. 2014 for details), we attributed each cluster star to RGB or AGB, identifying 87 RGB stars and 30 AGB stars. The position of the member stars on the V –($U - V$) CMD (and their attribution to RGB or AGB sequence) is shown in Figure 3. Note that attribution to a given evolutionary sequence of the bluest stars brighter than $V \sim 16.6$ is not trivial. Five stars with $V < 16.6$ are labeled as AGB stars but we cannot exclude that they are actually RGB stars.

7. The Iron Spread

We used the maximum likelihood (ML) algorithm described in Mucciarelli et al. (2012) to estimate whether the observed scatter measured in the iron abundance is compatible or not with a null intrinsic spread, taking into account the uncertainties of individual stars. Iron abundances and corresponding uncertainties are listed in Tables 3 and 4 for UVES and GIRAFFE targets respectively. We checked different subsamples of member stars.

1. Total sample (117 stars): the ML algorithm provides an average value of $[\text{Fe}/\text{H}] = -2.14 \pm 0.01$ dex with an intrinsic spread of 0.02 ± 0.01 dex (the observed scatter

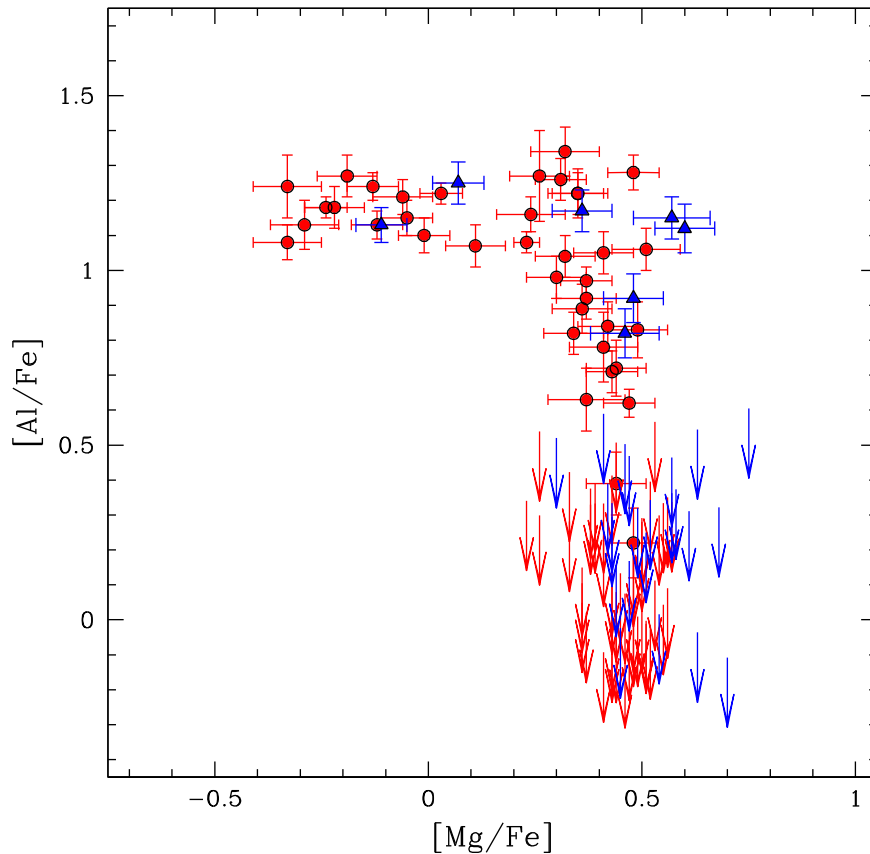


Figure 5. Behavior of $[Al/Fe]$ as a function of $[Mg/Fe]$ for the member stars of NGC 5824. Arrows indicate upper limits for $[Al/Fe]$. Red and blue symbols are for the RGB and AGB stars, respectively.

is 0.07 dex). This result suggests the presence of a small abundance spread.

2. RGB stars (87 stars): the average $[Fe/H]$ of the RGB stars only is -2.11 ± 0.01 dex with an observed scatter of 0.06 dex and an intrinsic spread of 0.00 ± 0.01 dex.
3. AGB stars (30 stars): the average $[Fe/H]$ of the AGB stars only is -2.20 ± 0.01 dex with an intrinsic spread of 0.00 ± 0.01 dex and an observed scatter of 0.07 dex. If we exclude from the AGB sample the five brightest AGB stars with doubtful attribution the derived abundance and intrinsic scatter do not change significantly.
4. RGB stars in common with DC14 (66 stars): 66 out of 88 stars in common with DC14 belong to RGB and they provide $[Fe/H] = -2.12 \pm 0.01$ dex with an intrinsic scatter of 0.00 ± 0.02 dex.

Even if the total sample seems to suggest a small (but marginally significant) iron dispersion (0.02 ± 0.01 dex), when the samples of RGB and AGB stars are analyzed separately they provide a clear lack of intrinsic scatter, indicating that the cluster has a homogeneous iron content (as already pointed out by Ro16). AGB and RGB stars show a systematic difference in their $[Fe/H]$ abundance ratios of about 0.1 dex, with the AGB stars having a lower abundance than the RGB stars. Figure 4 shows the $[Fe/H]$ distribution derived for the RGB and AGB samples, the red and blue histograms respectively, where the systematic offset between the two distributions is clearly visible. This finding agrees with the chemical analyses of AGB stars in other GCs (Lapenna et al. 2014, 2015, 2016; Mucciarelli et al. 2015a) that show a systematic (but still unexplained) underestimate of $[Fe/H]$ in AGB stars with

respect to the RGB stars of the cluster when the neutral iron lines are used. This difference between the iron abundances of RGB and AGB stars explains why the entire sample of cluster member stars provides a small iron dispersion (which totally disappears when the two groups of stars are analyzed independently).

8. Light Element Abundances: O, Na, Mg, Al

We investigated the occurrence in NGC 5824 of chemical anomalies in the abundances of O, Na, Mg, and Al. As suggested by Ro16, NGC 5824 has a star-to-star dispersion in the $[Mg/Fe]$ abundance larger than that usually observed in most GCs (see, e.g., Carretta et al. 2009c; Meszaros et al. 2015; Pancino et al. 2017). Figure 5 shows the behavior of $[Al/Fe]$ as a function of $[Mg/Fe]$ as obtained from our study. Mg abundances are available for all the member stars, and true measurements of Al have been obtained only for 45 stars, while for the other targets upper limits are provided, due to the weakness of the Al lines. A large spread is observed in both $[Mg/Fe]$ and $[Al/Fe]$, with $[Mg/Fe]$ ranging from enhanced values down to subsolar values (the minimum abundance is ~ -0.35 dex). On the other hand, $[Al/Fe]$ ranges over more than 1 dex. A clear Mg–Al anticorrelation is observed, with all the stars with $[Mg/Fe] < +0.15$ dex having $[Al/Fe] \sim +1.2$ dex.

Direct evidence of this strong anticorrelation is visible in Figure 6, where the spectra of two stars observed with GIRAFFE (namely #16286 and #21987) and of two stars observed with UVES (namely #35432 and #24182) are compared around the Mg and Al lines. The stars of each pair

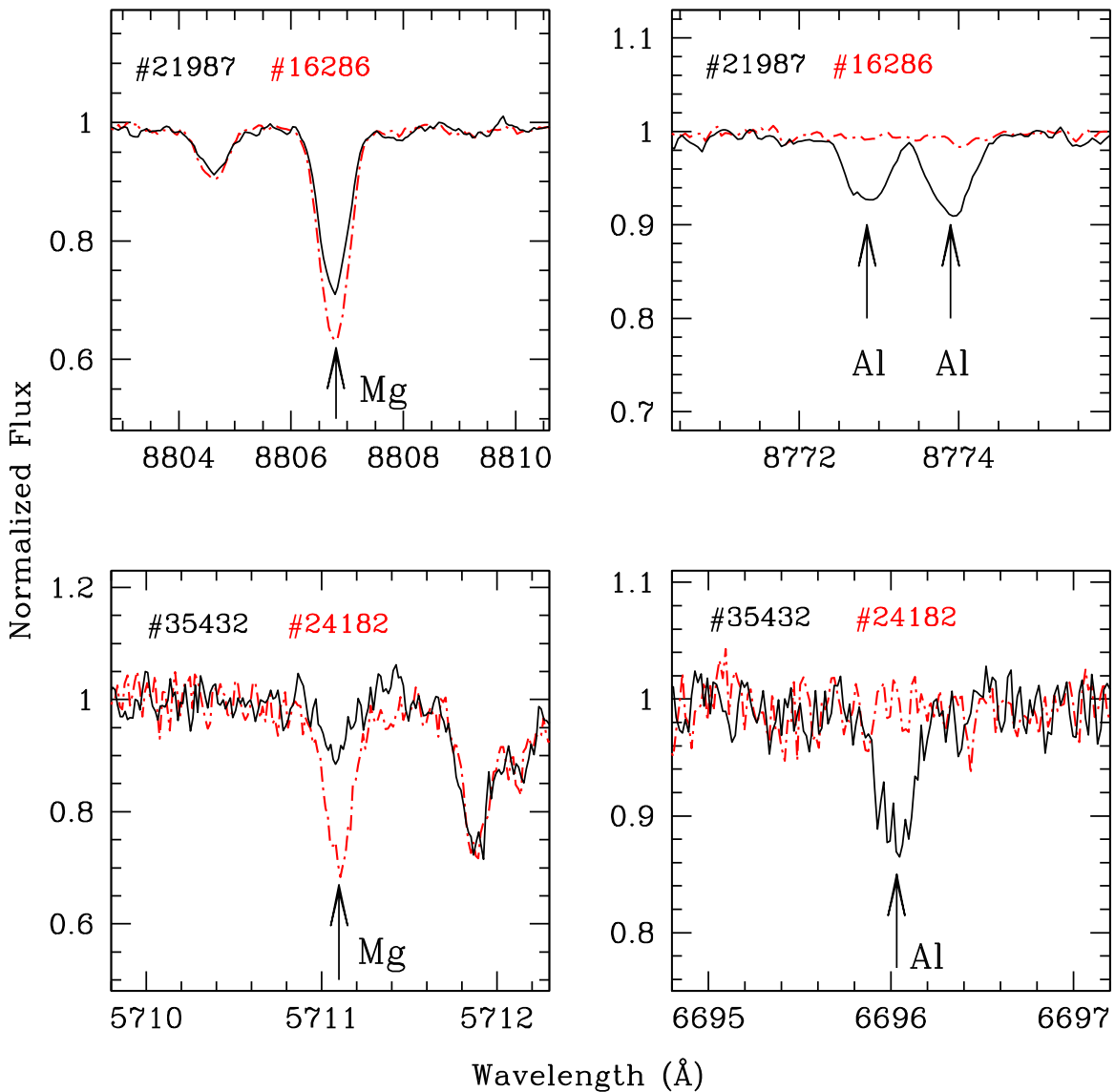


Figure 6. Portions of the spectra of the GIRAFFE stars #16286 and #21987 (upper panels), and of the UVES stars #35432 and #24182 (lower panels), around Mg and Al lines. The stars of both pairs have very similar atmospheric parameters.

have been selected in order to have very similar atmospheric parameters. The star #16286 shows a prominent Mg line but a total lack of Al lines, while for the star #21987 the situation is the opposite, with a weaker Mg line than the other star but clearly visible Al lines. The same situation is observed for the two UVES targets but using different Mg and Al features. The atmospheric parameters of the stars in each pair are very similar, so the different strengths observed in Mg and Al lines can be ascribed only to differences in abundance.

For the UVES targets we can also measure O and Na abundances. Figure 7 shows the behavior of the $[\text{Na}/\text{Fe}]$ abundance ratio for the six RGB stars observed with UVES as a function of $[\text{O}/\text{Fe}]$ (red points) in comparison with the stars measured in 19 Galactic GCs by Carretta et al. (2009b, 2009c). The six stars show a clear anticorrelation that matches well with that observed in other Galactic GCs.

9. Comparison with Da Costa et al. (2014)

The adopted GIRAFFE setup allows us to measure also the Ca II triplet lines, used by DC14 to infer an indirect estimate of

the iron content of the cluster. Similar to what they did, we measured the EWs of the two strongest Ca II lines (8542 and 8662 Å) for the cluster member stars, adopting a Voigt profile in order to reproduce the damped wings of these lines. $[\text{Fe}/\text{H}]$ has been derived using the calibration provided by Saviane et al. (2012) and adopting a reference horizontal branch magnitude $V_{\text{HB}} = 18.50$ as quoted by DC14. For the stars in common with DC14 we find a mean difference in the sum of the EWs of the two Ca II lines of $+0.03 \pm 0.01$ Å ($\sigma = 0.13$ Å). Such a small offset rules out the existence of any significant difference between the two studies, since a variation of 0.03 Å in the summed EW translates to a difference in $[\text{Fe}/\text{H}]$ of about 0.01 dex.

The uncertainties in $[\text{Fe}/\text{H}]$ derived from Ca II triplet lines have been estimated considering three sources of errors: (i) the uncertainty in the fitting procedure of the Ca II lines, (ii) that in the continuum location, and (iii) that related to the adopted EW- $[\text{Fe}/\text{H}]$ calibration. The first two sources have been estimated by using Monte Carlo simulations and analyzing samples of 500 synthetic spectra each with different S/N, and

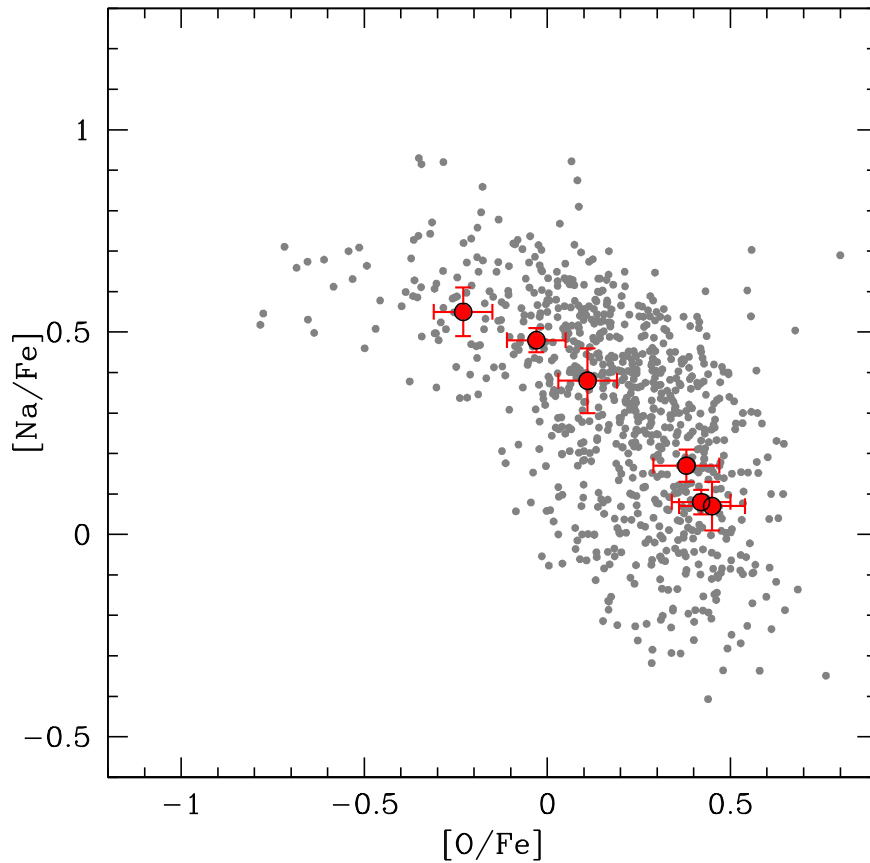


Figure 7. Behavior of $[\text{Na}/\text{Fe}]$ as a function of $[\text{O}/\text{Fe}]$ for the six RGB stars of NGC 5824 observed with UVES (red circles) in comparison with the Galactic GC stars (gray circles) analyzed by Carretta et al. (2009b, 2009c).

adopting the spectral resolution and pixel size of the HR21 GIRAFFE setup. The uncertainty in the EW– $[\text{Fe}/\text{H}]$ calibration by Saviane et al. (2012) has been estimated considering the global residual of their fit (~ 0.13 dex) normalized to the root mean square of the number of GCs used to derive the relation. The total uncertainties range from ~ 0.09 to 0.10 dex for the faintest targets to ~ 0.04 dex for the brightest ones.

The average $[\text{Fe}/\text{H}]$ abundance derived from the 81 RGB stars observed with GIRAFFE and for which we measured the Ca II lines strength is -1.99 ± 0.01 dex with an intrinsic scatter of 0.02 ± 0.01 dex, as derived adopting the ML approach. When we consider only the RGB stars in common with DC14 (60 in total) the average abundance is $[\text{Fe}/\text{H}] = -1.99 \pm 0.01$ dex with an intrinsic scatter of 0.00 ± 0.01 dex.

When the iron abundances of the entire sample of 108 RGB stars studied by DC14 are analyzed with the ML approach, an average abundance of -2.01 ± 0.01 dex is found, with an intrinsic spread of 0.05 ± 0.01 dex, suggesting a small but not negligible iron spread, at variance with the result obtained with our data set. In this test the uncertainties in EWs quoted by DC14 have been transformed into $[\text{Fe}/\text{H}]$ errors according to the relation of Saviane et al. (2012). The uncertainties in their $[\text{Fe}/\text{H}]$ have been re-derived using the same procedure described above: samples of synthetic spectra with different S/N between 50 and 130 (see Figure 11 in DC14) have been simulated, including a spectral resolution of ~ 2500 and a pixel size of 0.8 \AA per pixel, in order to simulate spectra similar to those obtained with FORS2 by DC14. Figure 8 shows the behavior of the abundance errors (derived from the

uncertainties in EWs quoted by DC14) as a function of the V-band magnitude for the DC14 targets (gray circles). In comparison, the black line represents the uncertainties expected according to our Monte Carlo simulations. On average the Monte Carlo uncertainties are systematically higher than those quoted by DC14.

When the new set of errors is adopted, the ML algorithm provides an intrinsic spread of 0.01 ± 0.02 dex, similar to what we obtained with the $[\text{Fe}/\text{H}]$ derived from the Ca II triplet measured with GIRAFFE spectra, but in contrast to the result obtained with the uncertainties of DC14. This finding suggests that the small iron spread obtained by DC14 was probably due to an underestimate of the uncertainties in the EWs of the Ca II lines. It is worth noting that the observed scatter of the $[\text{Fe}/\text{H}]$ distribution of the DC14 study is quite small and comparable with the scatters usually observed in GCs studied with high spectral resolution (with scatter smaller than 0.05 – 0.06 dex, see Carretta et al. 2009a).

Because of the large spread in $[\text{Mg}/\text{Fe}]$ found in NGC 5824 and not observed in most GCs, we check for possible correlations between the iron abundance derived from the Ca II lines and $[\text{Mg}/\text{Fe}]$. In fact, Mg plays a relevant role in the opacity of the atmospheres of giant stars, being one of the most important electron donors. A significant depletion in the Mg abundances leads to a decrease of the H^- opacity and of the electronic pressure, thus increasing the line strength of the Ca II lines (at a constant Fe and Ca abundance). This effect has been revealed for the first time in the GC NGC 2419 (Mucciarelli et al. 2012), where the unusual Mg depletion (down to $[\text{Mg}/\text{Fe}] \sim -1$ dex) observed in some cluster stars leads to a

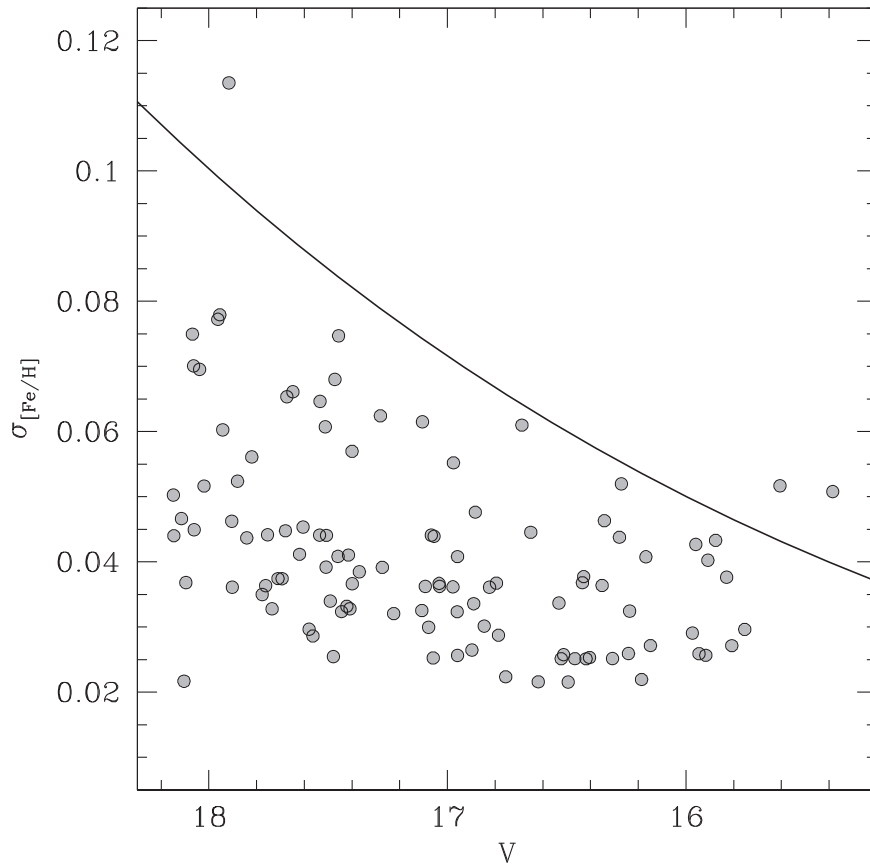


Figure 8. Behavior of [Fe/H] uncertainties from DC14 as a function of the V-band magnitude (gray points) in comparison with the expected uncertainty according to our Monte Carlo simulations (black line).

significant increase in the EWs of the Ca II lines, and that can be erroneously interpreted as a high Fe abundance.

Figure 9 shows the behavior of [Fe/H] (as derived from Ca II lines) as a function of [Mg/Fe] considering RGB stars only measured from our sample (upper panel) and from that of DC14 (lower panel). Both data sets show a mild anticorrelation between [Fe/H] and [Mg/Fe] in the expected sense: the stars with low [Mg/Fe] have systematically higher [Fe/H] abundances (solid lines in Figure 9 show the best linear fit to the data). The Spearman correlation test provides probabilities that the variables are uncorrelated of 0.01 from our sample and of 0.06 from the [Fe/H] of DC14. The probability of correlation increases when the [Fe/H] inferred from the GIRAFFE spectra are used, likely due to the higher spectral resolution and S/N than the data set of DC14 (which have S/N between 50 and 120, while those of the spectra of this study are between 70 and 250). This finding contradicts the analog test performed by Ro16 that found a low probability of correlation between their [Mg/Fe] and the [Fe/H] provided by DC14. Such a difference is likely due to the greater uncertainty of the [Mg/Fe] derived by Ro16 (the typical S/N of their spectra is 40–50) and of the [Fe/H] of DC14 with respect to this study.

The above correlation is weak and the few Mg-poor stars do not significantly change the observed scatter: when the stars with subsolar [Mg/Fe] are excluded, the dispersion in the average [Fe/H] decreases from 0.06 to 0.05 dex with both the data sets. However, the detection of this anticorrelation (using two independent sets of Ca II line strengths) confirms that metallicities inferred from Ca II lines could be overestimated in Mg-poor stars, and in general could be biased in the case of

anomalous and/or exotic chemical compositions (such as in NGC 2419).

10. Comparison with Roederer et al. (2016)

Twenty-three stars of our spectroscopic sample are in common with that of Ro16. When we compare the atmospheric parameters of these targets we find a significant difference in the adopted T_{eff} scales, with a difference (our study – Ro16) of +139 K ($\sigma = 45$ K). The average difference for the gravity is +0.09 ($\sigma = 0.03$) and that for v_t is +0.00 km s⁻¹ ($\sigma = 0.26$ km s⁻¹). Ro16 estimated the atmospheric parameters with an approach similar to that followed in our analysis, deriving T_{eff} and $\log g$ from the photometry, but constraining v_t spectroscopically (while we adopted the $\log g-v_t$ calibration of Kirby et al. 2009).⁷ The slightly lower $\log g$ found by Ro16 are compatible with the lower T_{eff} that they adopted. This difference in T_{eff} also explains the difference in the derived Fe abundances, with an average difference of +0.23 dex ($\sigma = 0.07$ dex). In their discussion of the metallicity of NGC 5824, Ro16 used [Fe II/H] because they found a large (~ 0.4 dex) difference between Fe abundances from neutral and singly ionized lines, with [Fe I/H] systematically lower than [Fe II/H]. As a check, we reanalyzed the stars in common with Ro16, adopting their

⁷ Even if we adopted the same photometric magnitudes, $E(B - V)$, extinction coefficients, and transformation between photometric systems adopted by Ro16, we are not able to reproduce the T_{eff} quoted in their Table 1. We note that the only way to recover the same values is to assume $E(B - V) = 0.07$ mag instead of the quoted value of $E(B - V) = 0.14$ mag.

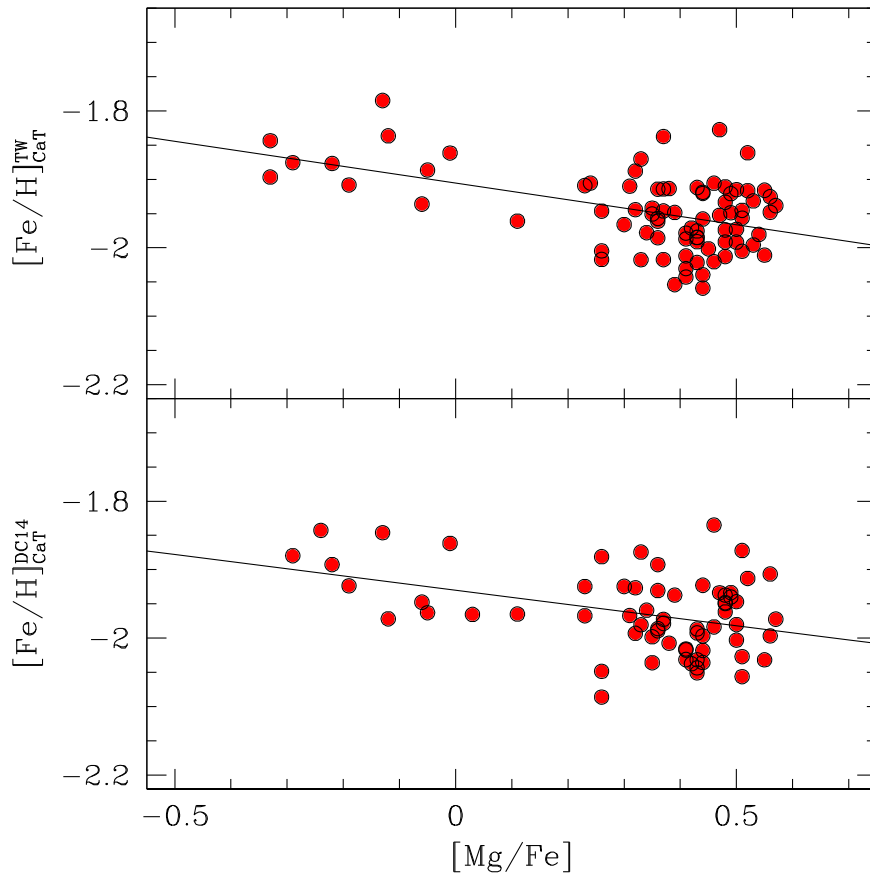


Figure 9. Behavior of $[\text{Fe}/\text{H}]$ as derived from the Ca II triplet lines (from this work in the upper panel, and from DC14 in the lower panel) as a function of $[\text{Mg}/\text{Fe}]$. Solid gray lines are the linear best fits.

atmospheric parameters and finding $[\text{Fe I}/\text{H}] = -2.29 \pm 0.02$ dex ($\sigma = 0.08$ dex) and $[\text{Fe II}/\text{H}] = -2.07 \pm 0.01$ dex ($\sigma = 0.02$ dex, only for the six UVES stars). They attributed the observed difference between $[\text{Fe I}/\text{H}]$ and $[\text{Fe II}/\text{H}]$ to the fact that Fe I lines can be less reliable diagnostics than Fe II lines in metal-poor giant stars (for instance due to the occurrence of non-local thermodynamic equilibrium). We think that the difference measured between the two abundance ratios is instead due to an underestimate of the adopted temperatures. This is confirmed by the reanalysis of the UVES targets using the Ro16 T_{eff} , that providing significant positive slopes between the iron abundance and the excitation potential, indicating an underestimate of T_{eff} . On the other hand, our photometric T_{eff} for the UVES stars do not require adjustment to reproduce the excitation equilibrium.

The derived $[\text{Mg}/\text{Fe}]$ distribution is compatible with that obtained by Ro16. Ro16 found a large difference (~ 0.4 dex) between the Mg abundances derived from two stars observed both with M2FS (using the Mg I line at 4571.1 Å) and MIKE (where abundances are based on three optical lines), probably due to departures from local thermodynamic equilibrium that could affect that blue transition at 4571.1 Å arising from the ground level of the Mg I atom. Following the suggestion by Ro16, we increase by 0.4 dex all their abundances derived from M2FS spectra, finding an average difference for the stars in common between our study and theirs of $+0.10 \pm 0.03$ dex ($\sigma = 0.15$ dex). Despite possible offsets between the two abundance scales, the ranges of $[\text{Mg}/\text{Fe}]$ in the two studies, based on different Mg transitions, are fully compatible,

confirming the large depletion of $[\text{Mg}/\text{Fe}]$ in some stars of NGC 5824.

11. Conclusions

From the analysis of FLAMES high-resolution spectra of 117 giant-star members of the GC NGC 5824 we obtained two main results, namely (1) the lack of spread in the iron abundance, and (2) the detection of an extended Mg–Al anticorrelation.

The cluster has an average iron abundance of -2.11 ± 0.01 dex when we consider the sample of 87 bona-fide RGB stars. This sample does not show any evidence of intrinsic spread, confirming the first claim by Ro16 (which analyzed 26 stars with $V < 17$) but based on a larger sample. According to this finding, NGC 5824 turns out to be a *normal* GC, showing no evidence of internal self-enrichment in terms of iron, hence there is no reason to consider it the remnant of a complex stellar system (such as a dwarf spheroidal galaxy). On the other hand it does not show any significant evidence of chemical peculiarities (such as spread in s-process or C+N+O elements). In fact, although neither our data set nor that of Ro16 allowed direct measurement of C and N abundances, the optical CMDs of NGC 5824 (see Sanna et al. 2014; Walker et al. 2017) did not reveal any anomalous splitting of the subgiant branch (which has been interpreted as evidence of an intrinsic C+N+O spread, see Piotto et al. 2012). Also, as shown by Ro16, no star-to-star variation in s-process elements is found in NGC 5824, with the sole exception of one star in Ro16’s sample that exhibits a systematic enhancement of the

s-process elements. This star is present also in our sample (the UVES target #24182): we found the same enhancement of the s-process lines with respect to the other five UVES targets (no s-process transitions are available in the GIRAFFE spectra). However, this star shows an iron abundance fully compatible with the other stars, in contrast to the other anomalous GCs where the most metal-rich stars exhibit higher s-process abundances.

The present sample also allows us to detect the occurrence of the standard signature of multiple populations in GCs, the Na–O anticorrelation. Additionally, we detect a very extended Mg–Al anticorrelation. At variance with the Na–O anticorrelation that is observed in all the old GCs in our Galaxy and in other galaxies of the Local Group, the Mg–Al anticorrelation turns out to be present in only a few clusters. This is likely due to the different temperatures needed to ignite the NeNa cycle (responsible for the Na–O anticorrelation, $T \sim 50$ MK) and the MgAl cycle (responsible for the Mg–Al anticorrelation, $T \sim 70$ MK).

First Carretta et al. (2009c) proposed that the spread in [Al/Fe] and the extension of the Mg–Al anticorrelation are driven by two main parameters, namely the present-day cluster mass and the metallicity. Subsequent analyses by Meszaros et al. (2015) and Pancino et al. (2017) confirmed this behavior. The spread in [Al/Fe] decreases, increasing the metallicity, with the most metal-rich and low-mass GCs showing little or no spread in [Al/Fe] (see the cases of M4 (Carretta et al. 2009c) and NGC 6362 (Massari et al. 2017)). Well-developed Mg–Al anticorrelations have been found in metal-poor GCs (NGC 4833, M15, M92) or in high-mass GCs with intermediate (NGC 6752, M13) or high metallicity (NGC 2808). Pancino et al. (2017) show that the spread in [Al/Mg] abundance ratio clearly increases with the present-day mass and decreases with metallicity. Also, Mg-poor stars (with [Mg/Fe] < +0.1 dex) have been found in NGC 2419 (Cohen & Kirby 2012; Mucciarelli et al. 2012), in M54 (Carretta et al. 2010b), and in Omega Centauri (Norris & Da Costa 1995), the most metal-poor, massive GC-like systems.





NGC 5824 well fits into this framework, being the 14th most luminous GC (according to the 2010 edition of Harris 1996) and the third most luminous GC among those with [Fe/H] < –1.9 dex, after NGC 2419 and M15 (both of which show a large [Mg/Fe] spread but homogeneous [Fe/H]).

This behavior of the [Al/Fe] and [Mg/Fe] spreads with the metallicity is in principle compatible with the scenario where the main polluters are the high-mass AGB stars of the first GC stellar generation that can activate the MgAl cycle during hot bottom burning. At low metallicity the AGB stars can activate the hot bottom burning at lower masses (Ventura et al. 2011, 2013, 2016). On the other hand, massive GCs, even at high metallicity, have deeper potential wells and they can more efficiently retain the polluter ejecta (as in the case of NGC 2808).

We conclude that NGC 5824 is a standard GC, without spread in [Fe/H] and with the presence of the usual chemical anomalies (both Na–O and Mg–Al anticorrelations), but showing a large (and rare) spread in Mg.

We thank the referee, Luca Sbordone, for his useful suggestions and comments.

ORCID iDs

Alessio Mucciarelli  <https://orcid.org/0000-0001-9158-8580>
 Emilio Lapenna  <https://orcid.org/0000-0002-7662-2186>
 Francesco R. Ferraro  <https://orcid.org/0000-0002-2165-8528>
 Barbara Lanzoni  <https://orcid.org/0000-0001-5613-4938>

References

- Alonso, A., Arribas, S., & Martinez-Roger, C. 1999, *A&AS*, 140, 261
 Alonso, A., Arribas, S., & Martinez-Roger, C. 2001, *A&AS*, 376, 1039
 Bastian, N., & Lardo, C. 2015, *MNRAS*, 453, 357
 Bekki, K., & Freeman, K. C. 2003, *MNRAS*, 346, L11
 Bellazzini, M., Ibata, R. A., Chapman, S. C., et al. 2008, *AJ*, 136, 1147
 Brown, J. A., Wallerstein, G., & Gonzalez, G. 1999, *AJ*, 118, 1245
 Caffau, E., Ludwig, H.-G., Steffen, M., Freytag, B., & Bonifacio, P. 2011, *SoPh*, 268, 255
 Carretta, E., Bragaglia, A., Gratton, R., D’Orazi, V., & Lucatello, S. 2009a, *A&A*, 508, 695
 Carretta, E., Bragaglia, A., Gratton, R., et al. 2009b, *A&A*, 505, 117
 Carretta, E., Bragaglia, A., Gratton, R., & Lucatello, S. 2009c, *A&A*, 505, 139
 Carretta, E., Bragaglia, A., Gratton, R. G., et al. 2010a, *ApJ*, 714L, 7
 Carretta, E., Bragaglia, A., Gratton, R. G., et al. 2010b, *A&A*, 520, 95
 Carretta, E., Bragaglia, A., Gratton, R. G., et al. 2014, *A&A*, 561, 87
 Castelli, F. 2005, *MSAIS*, 8, 44
 Castelli, F., & Kurucz, R. L. 2004, arXiv:astro-ph/0405087
 Cayrel, R. 1988, in IAU Symp. 132, The Impact of Very High S/N Spectroscopy on Stellar Physics, ed. G. Cayrel de Strobel & M. Spite (Dordrecht: Kluwer Academic), 345
 Cohen, J. G., & Kirby, E. N. 2012, *ApJ*, 760, 86
 Da Costa, G. S., Held, E. V., & Saviane, I. 2014, *MNRAS*, 438, 3507
 Dekker, H., D’Odorico, S., Kaufer, A., Delabre, B., & Kotzlowski, H. 2000, *Proc. SPIE*, 4008, 534
 Ferraro, F. R., Dalessandro, E., Mucciarelli, A., et al. 2009, *Natur*, 462, 483
 Ferraro, F. R., Massari, D., Dalessandro, E., et al. 2016, *ApJ*, 828, 75
 Ferraro, F. R., Messineo, M., Fusi Pecci, F., et al. 1999, *AJ*, 118, 1738
 Gratton, R. G., Carretta, E., Eiríksson, K., & Gustafsson, B. 1999, *A&A*, 350, 1065
 Grevesse, N., & Sauval, A. J. 1998, *SSR*, 85, 161
 Harris, W. E. 1996, *AJ*, 112, 1487
 Ibata, R., Sollima, A., Nipoti, C., et al. 2011, *ApJ*, 738, 186
 Johnson, C. I., Caldwell, N., Rich, R. M., Pilachowski, C. A., & Hsyu, T. 2016, *AJ*, 152, 21
 Johnson, C. I., & Pilachowski, C. A. 2010, *ApJ*, 722, 1373
 Kirby, E. N., Guhathakurta, P., Bolte, M., Sneden, C., & Geha, M. 2009, *ApJ*, 705, 328
 Lapenna, E., Lardo, C., Mucciarelli, A., et al. 2016, *ApJ*, 826L, 1
 Lapenna, E., Mucciarelli, A., Ferraro, F. R., et al. 2015, *ApJ*, 813, 97
 Lapenna, E., Mucciarelli, A., Lanzoni, B., et al. 2014, *ApJ*, 797, 124
 Lardo, C., Mucciarelli, A., & Bastian, N. 2016, *MNRAS*, 457, 51
 Marino, A. F., Milone, A. P., Piotto, G., et al. 2009, *A&A*, 505, 1099
 Marino, A. F., Milone, A. P., Karakas, A. I., et al. 2015, *MNRAS*, 450, 815
 Marino, A. F., Sneden, C., Kraft, R. P., et al. 2011a, *A&A*, 532, 8
 Marino, A. F., Milone, A. P., Piotto, G., et al. 2011b, *ApJ*, 731, 64
 Massari, D., Mucciarelli, A., Dalessandro, E., et al. 2017, *MNRAS*, 468, 1249
 Massari, D., Mucciarelli, A., Ferraro, F. R., et al. 2014, *ApJ*, 795, 22
 McCall, M. L. 2004, *AJ*, 128, 2144
 Meszaros, S., Martell, S. L., Shetrone, M., et al. 2015, *AJ*, 149, 153
 Mucciarelli, A. 2013, arXiv:1311.1403
 Mucciarelli, A., Bellazzini, M., Ibata, R., et al. 2012, *MNRAS*, 426, 2889
 Mucciarelli, A., Bellazzini, M., Ibata, R., et al. 2017a, *A&A*, 605, 46
 Mucciarelli, A., Lapenna, E., Massari, D., Ferraro, F. R., & Lanzoni, B. 2015a, *ApJ*, 801, 69
 Mucciarelli, A., Lapenna, E., Massari, D., et al. 2015b, *ApJ*, 809, 128
 Mucciarelli, A., Monaco, L., Bonifacio, P., & Saviane, I. 2017b, *A&A*, 603, L7
 Mucciarelli, A., Pancino, E., Lovisi, L., Ferraro, F. R., & Lapenna, E. 2013, *ApJ*, 766, 78
 Norris, J. E., & Da Costa, G. S. 1995, *ApJ*, 447, 680
 Origlia, L., Ferraro, F. R., Bellazzini, M., & Pancino, E. 2003, *ApJ*, 591, 916
 Origlia, L., Massari, D., Rich, R. M., et al. 2013, *ApJ*, 779L, 5
 Origlia, L., Rich, R. M., Ferraro, F. R., et al. 2011, *ApJ*, 726L, 20
 Pancino, E., Mucciarelli, A., Sbordone, L., et al. 2011, *A&A*, 527, 18
 Pancino, E., Romano, D., Tang, B., et al. 2017, *A&A*, 601, 112

- Pasquini, L., Avila, G., Allaert, E., et al. 2000, [Proc. SPIE](#), **4008**, 129
- Pietrinferni, A., Cassisi, S., Salaris, M., & Castelli, F. 2006, [ApJ](#), **642**, 797
- Piotto, G., Milone, A. P., Anderson, J., et al. 2012, [ApJ](#), **760**, 39
- Renzini, A., D'Antona, F., Cassisi, S., et al. 2015, [MNRAS](#), **454**, 4197
- Roederer, I. U., Mateo, M., Bailey, J. I., et al. 2016, [MNRAS](#), **455**, 2417
- Sanna, N., Dalessandro, E., Ferraro, F. R., et al. 2014, [ApJ](#), **780**, 90
- Saviane, I., da Costa, G. S., Held, E. V., et al. 2012, [A&A](#), **540**, 27
- Sbordone, L., Bonifacio, P., Castelli, F., & Kurucz, R. L. 2004, [MSAIS](#), **5**, 93
- Simmerer, J., Ivans, I. I., Filler, D., et al. 2013, [ApJ](#), **764L**, 7
- Stetson, P. B., & Pancino, E. 2008, [PASP](#), **120**, 1332
- Venn, K. A., Irwin, M., Shetrone, M. D., et al. 2004, [AJ](#), **128**, 1177
- Ventura, P., D'Antona, F., Mazzitelli, I., & Gratton, R. G. 2011, [ApJL](#), **550**, L65
- Ventura, P., Di Criscienzo, M., Carini, R., & D'Antona, F. 2013, [MNRAS](#), **431**, 3642
- Ventura, P., Garcia-Hernandez, D. A., Dell'Agli, F., et al. 2016, [ApJ](#), **831**, 17
- Villanova, S., Geisler, D., Carraro, G., Moni Bidin, C., & Munoz, C. 2013, [ApJ](#), **778**, 186
- Walker, A. R., Andreuzzi, G., Martinez-Vasquez, C. E., et al. 2017, [AJ](#), **154**, 8
- Willman, B., & Strader, J. 2012, [AJ](#), **144**, 76
- Yong, D., Roederer, I. U., Grundahl, F., et al. 2014, [MNRAS](#), **441**, 3396